Inter-Individual Variability in Brain Function Captured by a Siamese Neural Network

Bea Waelbers
s4591704
b.waelbers@student.ru.nl

Thesis MSc Cognitive Neuroscience – SOW-DGCN05
Radboud University, Nijmegen, the Netherlands

Supervisors: dr. Linda Geerligs & dr. Umut Güçlü
Second Reader: dr. Tim Kietzmann

Abstract

Neuroscience has focused on group differences for a long time. However, individual variability can be important for explaining and predicting brain disorders and age-related changes. Here, we will investigate these inter-individual differences by using data from the Human Connectome Project. Two resting-state fMRI time series will be inputted to a Siamese neural network that will learn whether the two inputs are from the same person, or from two differing persons. We show that it can do this with an accuracy of 93%. The features learned by the network showed clear links to known large-scale brain networks. We found 1) a higher-level network component with correlations to lower-level networks, 2) an intra-network component, and 3) a higher-level network component without correlations to lower-level networks. The first component, in particular the default mode network, the dorsal attention network and the cinguloopercular network, showed an association with fluid intelligence, speed of processing, language comprehension and emotion recognition. The intra-network component showed a link with cognitive tests such as episodic memory, cognitive flexibility and speed, language, intelligence and emotion recognition. So, we showed that we can identify a low-dimensional representation of inter-individual variability of brain function by using a Siamese neural network, where the features can be linked to large-scale neural network and cognitive function.

Keywords: functional connectivity, Siamese neural networks, resting state, fMRI

1. Introduction

Brain connectivity specifies how different neurons, groups of neurons or even brain regions are connected and can be expressed by the pattern of anatomical networks [structural connectivity], by the causal interactions [effective connectivity], or by the temporal correlation between spatially defined brain regions [functional connectivity] (Friston, 1994; Friston, 2011). To study functional brain connectivity, functional magnetic resonance imaging (fMRI) measured in resting state (rs-fMRI or R-fMRI) is used most often (Damoiseaux et al., 2006). Resting-state data is acquired when a participant is laying in the scanner without a task. So, the brain mapping relates to a task-negative state, where the spontaneous fluctuations in brain activity are obtained. By correlating these spontaneous fluctuations in blood oxygen level dependent (BOLD) signal change over brain regions, the functional brain connectivity is computed, also called the intrinsic connectivity. Brain regions that are highly correlated are said to form a resting state network. These networks are established in multiple studies (Beckmann et al., 2005, Damoiseaux et al., 2006; Smith et al., 2009; Smitha et al., 2019). Some example networks are the primary visual network, the auditory network, and the default mode network. The default mode network (DMN) is an important resting state network, since this network's activity increases in resting state compared to most task states (Van den Heuvel & Hulshoff Pol, 2010). Resting state networks are found to be consistent over different

states of consciousness (fully awake, asleep, and under anesthesia (Smith et al. 2013)) and over different subjects, making them a robust measure of brain function.

1.1 Group comparisons

Neuroscience has been interested in comparing different groups of people in order to get a better understanding of the similarities and differences between these groups. One important comparison that is often made is healthy brains versus people with a certain brain disorder. For example, functional connectivity of patients with Alzheimer's disease have been compared to healthy control subjects (Wang et al., 2006). It has also been used to identify patients with major depression (Zeng et al., 2012), schizophrenia (Lynall et al., 2010) and Parkinson's disease (Amboni et al, 2015). Another domain in neuroscience that uses group comparisons is the field of aging, where the functional connectivity profiles of young and old adults are compared (Balsters et al., 2013; Geerligs et al., 2014). Most studies focus on the group differences that are present in the majority of participants, while ignoring variability between individuals within each group. However, these inter-individual differences have been shown to be related to higher cognitive functions (Mohr & Nagel, 2010; Kanai & Rees, 2011). By looking at single subject brain data, individual-specific features, which are reliable both within subjects and between subjects, can be discovered (Gordon, 2017). By computing functional connectivity profiles from resting state data, Finn et al. (2015) showed a stable "fingerprint". The term "neural fingerprint' is a reference to the human fingerprint, which is unique for every single person. This functional connectivity profile is shown to be stable over months to years (Chen et al., 2015, Horien et al., 2019), making it a reliable aspect of brain connectivity. The "neural fingerprint" is a robust and reliable way to identify a particular person from a large group. It uses the many functional connections to identify a certain person. Functional connectivity profiles can be used to predict behavioral and neural scores. For example, the dorsal attention network (DAN) activity can be predicted from functional connectivity fingerprints (Osher et al., 2019). In addition, this neural 'fingerprint' can be used to predict cognitive functioning (Mars, Passingham & Jbabdi, 2018; Mansour et al., 2021). For example, the frontoparietal and medial frontal networks predict levels of fluid intelligence (Finn et al., 2015). Connectivity of the parietal cortex in the resting state network was also linked to intelligence (Langer et al., 2011). Gratton et al. (2018) showed that individual variability was more substantial in the control systems (namely cinguloopercular, frontoparietal, salience and attention networks) while state- and session-dependent variability were stronger in the sensorimotor processing systems. Recently, functional connectivity profiles have been suggested as clinical tool, in order to quantify the subjects' clinical phenotype (Smitha et al., 2019; Dimitri et al., 2021). By exploiting functional connectivity profiles, brain disorders and age-related changes in brain function might be identified earlier and more accurately.

1.2 Subject identification

By focusing on inter-individual variability, i.e., the differences in functional connectivity between different people, neuroscience might be able to better explain brain disorders and aging on an individual level. Therefore, research has focused on how individuals can be identified from a batch of subjects, by using the neural fingerprint discussed above. First, Mueller et al. (2012) used repeated-measurement rs-fMRI to investigate individual differences in functional connectivity. Higher-order areas showed higher variability compared to lower-order brain areas. Miranda-Dominguez et al. (2014) proposed a linear model where the activity of a regions was defined as the weighted sum of the adjacent regions in order to identify the functional fingerprint of participants. Individuals were identified by higher-order region connections, such as the frontal and parietal cortices. Yoo et al. (2019) used a multivariate approach, incorporating a multivariate distance correlation to measure the dependency of two sets of signals on a higher level. They suggest that

this multivariate approach leads to a more stable and reliable prediction on individual differences in behavior and cognition. Byrge et al. (2019) have investigated how many connections are necessary in a functional connectivity profile in order to identify individuals correctly. They showed that even with a small part of the functional connectivity profile, identification was high. Sripada et al. (2019) found approximately 50 to 150 components to explain this individual variability. This suggests that the high dimensionality of the connectivity profile can be represented by a low dimensionality representation, corresponding to only the most important inter-individual variability. Demeter et al. (2020) identified both individuals and their twin-sibling by training a learning algorithm, known as support vector machine classifiers. They showed not only classification within individuals, but also within families, resulting in a suggestion that these functional connectivity profiles show genetic properties. Despite the majority of the studies utilizing rs-fMRI data, identifying individuals has also been achieved for other types of imaging studies. Valizadeh et al. (2019) used EEG data combined with different types of functional and effective connectivity measures. They tried different machine learning techniques, such as neural networks, support vector machines and linear discriminant analysis. For the functional connectivity measures, participant identification was 98% accurate. Then, Da Silva Castanheira et al. (2021) used MEG to seek a similar neural fingerprint as by Finn et al. (2015). Again, they found a stable functional connectivity profile that can identify individuals with high accuracy, showing these functional connectivity profiles can be used over different imaging modalities.

1.3 Deep neural networks

Another technique that is upcoming in neuroscience is deep neural networks (DNNs). DNNs are an extension of artificial neural networks, consisting of an input layer, an output layer, and a dynamic number of hidden intermediate layers. The goal of a deep neural network is to learn specific features by adjusting its weights in order to predict the correct output from its input. To capture inter-individual differences in brain functioning, different types of DNNs can be exploited. Chen et al. (2018) used recurrent neural networks, combining both the spatial and temporal dimension of the fMRI data in order to identify subjects. They showed that by using 100 time frames, an accuracy of 94% was achieved. Dimitri et al. (2021) combined different imaging modalities for subject identification, in order to combine different types of information. Then, they performed a deep learning dimension reduction algorithm to get a compressed representation of the multimodal data. First, convolutional blocks were used to obtain the low-level features. In order to get the reconstructions of the images, a general adversarial network was used. The clustered latent representations mapped onto phenotypic information, such as neuropsychological and personality variables, in such a way that they can be used as a biomarker to help in disease identification, understanding and treatment.

Here, we will use a DNN to discriminate between people's resting state brain data. Then, we will examine the features learned by the DNN to see whether the learned features can be linked to large-scale brain networks and the cognitive scores of participants. In order to do so, a Siamese neural network (SNN) will be used. An SNN consists of two sister networks, that have the same weights and biases (see Figure 1). The outputs of these sister networks are then used to compute the similarity of the learned features by using a difference function.

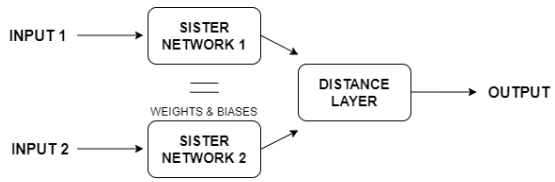

Figure 1: Siamese Neural Network architecture

SNNs rank the similarity between the inputs, meaning that two similar inputs will have an output close to 1. In contrast, very different inputs will result in an output close to 0 (Koch, Zemel & Salakhutdinov, 2015). SNNs are an important technique in the domain of image recognition. Here, the network receives two images and uses one-shot learning in order to determine whether the two images belong to the same class or not. SNNs have been used to automatically extract gait features for human identification (Zhang et al., 2016). Recently, research has shown that SNNs can be used to discriminate the same subject's connectivity profiles from other subjects that were recorded on the same day (Voorn, 2020). By computing the connectivity profiles of the resting state data from different participants, and using them as an input of an SNN, the network could discriminate whether it received two functional connectivity inputs from the same participant, or two inputs from different participants. Here we extend this research by examining the features learned by the hidden, intermediate layers of the network. Our aim is to get a better understanding of the individual differences in brain function and how they are associated with cognitive abilities. We will explore these characteristics by examining the features learned by the SNN when it is being trained on discriminating high-dimensional functional connectivity data of the same and different participants. The features learned by these networks can then be used as markers of variability between individuals. These markers are subsequently related to cognitive behavior, as discussed above. So, we will investigate whether we can generalize the established features of brain function that vary between individuals, obtained by a SNN, and link them to cognitive function.

2. Methods

2.1 Dataset and preprocessing

For this study, the Human Connectome Project (HCP) database was used. The dataset contains behavioral and genetic data, as well as data from multiple neuroimaging methods, namely structural MRI, resting-state fMRI (rs-fMRI), task fMRI (tfMRI) and diffusion MRI (dMRI) of 1200 participants (Van Essen et al., 2013). The population of the participants consists of twins and their non-twin siblings (age:22-35). Subjects were scanned on two successive days by a 3T scanning protocol. Participants with missing data for either of these days were removed, resulting in a dataset of 996 participants for this study. The HCP dataset's preprocessing pipelines are used, by using the Resting State fMRI 1 FIX-Denoised (Extended) and Resting State fMRI 2 FIX-Denoised (Extended) files (for more information, see Glasser (2013) and Van Essen (2013)). First, an independent component analysis (ICA) was implemented to correct for subject movement during scanning, where it removes noise that is structured and increases signal that has been lost during subject motion (Glasser et al., 2016). Next, a regression analysis was performed to remove the low frequency changes that are due to MR scanner drift. The parcellation scheme of Gordon (2016) was used to assign a neuroanatomical label to each location of the brain data. Regions of interest (ROIs) with less than 20 active voxels were removed, resulting in 332 remaining ROIs. For every subject, multiple connectivity profiles were computed. Every participant completed 4 rs-fMRI sessions on two days. Every session had a total of 1200, 0.72s during, TRs. Therefore, 4800 TRs were recorded per subject. In order to get sufficient data for training the model, multiple connectivity profiles were created for every subject, where 240 random volumes of the total time course of that subject were used to calculate the Pearson correlation coefficient. The upper triangle of the connectivity matrix was flattened and used as the input of the network. Finally, the dataset was divided into a validation set and test set, by randomly sampling participants. In order to not bias the model, it was trained on every participant for an equal number of steps, namely every third step, resulting in a validation set of 768 participants and a test set of 228 participants.

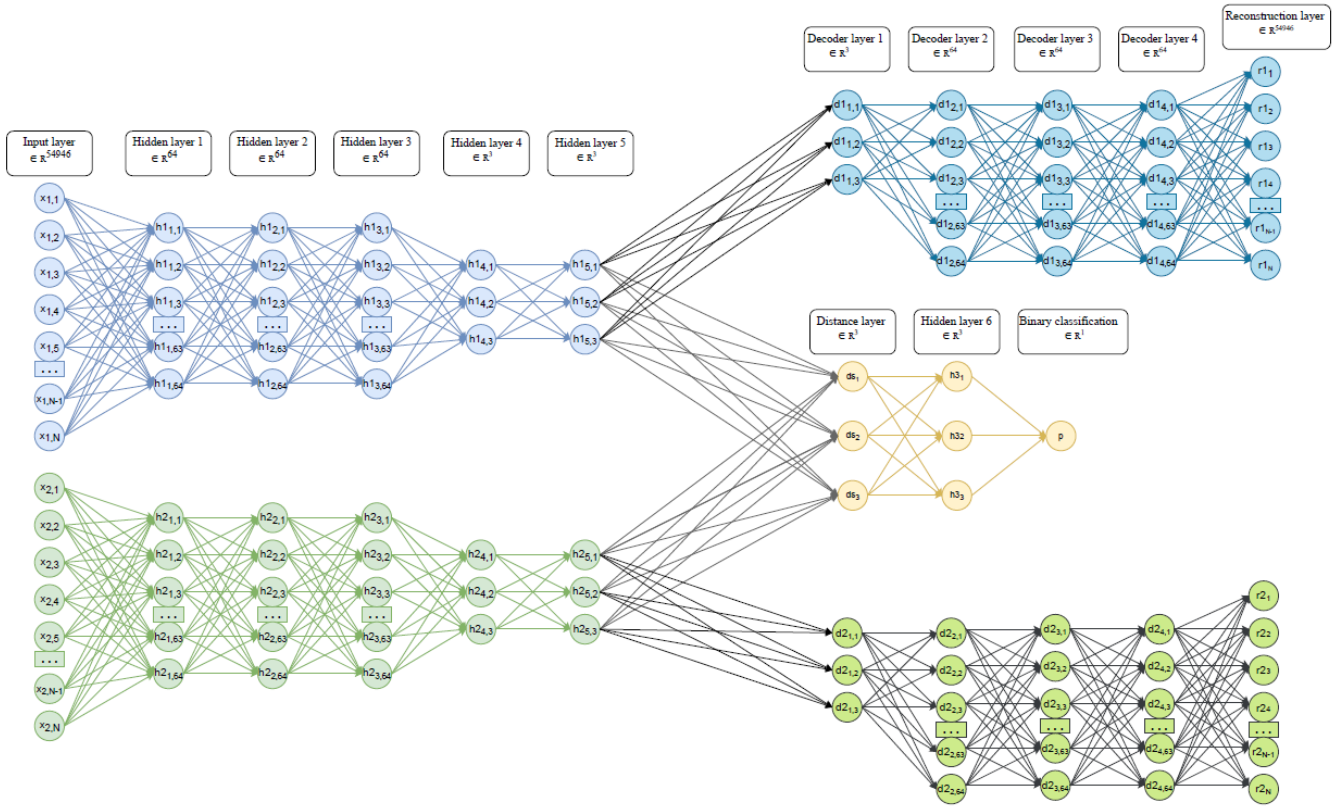

Figure 2: Neural network architecture. The left blue and green parts of the network are the two sister networks of the SNN. The outputs of these sister networks are combined in the distance layer, after which a prediction (same person or not) is made in the yellow part of the network. Next, both blue parts of the network are the first autoencoder, where the encoder part of the network corresponds to the first sister network of the SNN. The second part is the decoder part of the autoencoder, with mirrored layers compared to the encoder resulting in a reconstructed input. The green part is the second autoencoder. The first part corresponds to the second sister network. The second part is the decoder of the second autoencoder resulting again in a reconstructed input

2.2 Network architecture

Our deep neural network is a Siamese neural network (SNN). The SNN is used to predict whether the two connectivity profiles are from the same person or from a different person. So, the dimensionality of the input data is reduced. Then, an autoencoder is added. This autoencoder tries to reconstruct the original connectivity profiles. Because the autoencoder needs to use the compressed data to reconstruct the input, the network needs to learn the most important features of the input. Therefore, when training the Siamese neural network multiple times, adding an autoencoder enhances the stability of the features.

2.2.1 Siamese neural network

The siamese neural network consists of two components: two sister networks (see the left blue and left green part of Figure 2) and a merging part (the yellow part of Figure 2). The sister networks have the same weights and biases. First, the input layer has the size of the input, namely the upper triangle of the connectivity profiles (as discussed in *2.1 Dataset and preprocessing*), resulting in 54946 nodes. Then, hidden layer 1, 2 and 3 have 64 nodes. Hidden layer 4 and 5 have 3 nodes. All layers are fully-connected and feed-forward. The 3 nodes of hidden layer 5 are the features that we will use for further analysis. Neural networks are known for its hierarchical organization, with the first layers corresponding to lower-level features and the later layers corresponding to higher-level features. Since we want to analyze the features that are most likely to correspond to large-scale

brain networks, the features from hidden layer 5 will be used. So, both sister networks have an output layer of 3 nodes. Three output nodes are the least amount of output nodes possible to retain the performance levels of the network. Then, the outputs of these sister networks are combined by a distance layer, where the absolute difference is taken for the three output values of both sister networks. This distance layer is fully-connected to hidden layer 6, which also has 3 nodes. Then, there is a node for binary classification, which is a sigmoid function over the 3 output values of hidden layer. Here, the goal of the network is to discriminate the connectivity profiles of the same subject from other subjects. As discussed above, the model will have two inputs, for which there are two different options. The first option is that the two inputs are both from the same individual (target=1). Second, the inputs can be from different individuals (target=0). The output resulting from the SNN is the prediction of the network, namely a 0 (not the same person) or a 1 (the same person).

2.2.2 Autoencoder

An autoencoder consists of two components, namely an encoder and a decoder component. In the encoder component, the goal is to encode the input image by reducing its dimension. There, the left blue and green parts of Figure 2 present the encoders, where the blue one corresponds to sister network 1 of the SNN and the green one corresponds to sister network 2 of the SNN. The output layer of the encoder contains three nodes, which are the latent space representations of the input. The decoder component learns to reconstruct the original inputs as close as possible. The output of the encoder is the input of the decoder. Since we have two encoders (both sister networks of the SNN), there are also two decoders. The structure of the decoder is similar to the structure of the encoder. However, the number of nodes is mirrored, see Figure 2. So, the decoder part first has a layer with 3 nodes, namely decoder layer 1. Then, there are 3 hidden decoder layers with 64 nodes and an output layer, with 54946 nodes, corresponding to the size of the reconstructed input. Again, all layers are again fully-connected and feedforward.

2.2.3 Decorrelation penalty

In order to get independent features, a decorrelation term was added to the loss (Xiong et al. 2007). The decorrelation term is computed the following way. First, the outputs of the sister networks are normalized by taking the z-score. Next, the lower triangle of the correlation matrix of the normalized outputs is taken. Then, the Euclidean norm of the covariance matrix is subtracted by the diagonal of the covariance matrix (see *eq.1*). This penalty is multiplied by a constant factor Lambda and added to the loss of the model. The value of lambda is chosen by taking the smallest lambda that resulted in a correlation coefficient under 0.3 for all elements. Lambda was increased, starting from 0 with steps of 0.5, resulting in a lambda of 3.

$$L_{penalty} = \lambda \times \frac{1}{2}\left(||cov||_F^2 - \left||diag(cov)\right|\right|_F^2\right) \quad (eq.1)$$

2.2.4 Loss function

The loss function contains multiple components. First, the mean squared error is computed over the original input and the reconstructed input (see *eq.2*). Since there are two inputs (*i1* and *i2*) and two reconstructions (*r1* and *r2*), the resulting mean squared errors are averaged (see *eq.3*).

$$MSE = \frac{1}{n}\sum_{i=1}^{n}(Y_i - \hat{Y}_i)^2 \qquad (eq.2)$$

$$L_{reconstructions} = mean\big(MSE(i1, r1), MSE(i2, r2)\big) \quad (eq.3)$$

Next, the binary cross entropy is computed over the target and the prediction (see *eq.4*).

$$L_{prediction} = BCE = -\frac{1}{N}\sum_{i=1}^{N} y_i \times \log\big(p(y_i)\big) + (i - y_i) \times \log\big(1 - p(y_i)\big) \quad (eq.4)$$

Finally, the decorrelation term is added, resulting in the following loss:

$$\begin{aligned} L_{total} = {} & L_{reconstructions} \\ & + L_{prediction} \\ & + L_{penalty} \end{aligned} \qquad (eq.5)$$

2.3 Learning schedule

The model was implemented in Pytorch. The training phase of the model was terminated when the validation accuracy did not improve further and the correlation between the weights of the final hidden activation layer was below 0.3. Every epoch had 200 steps. The batch size was 256. Leaky ReLU was used as the activation function. The weights of the network were randomly initialized from a normal distribution. The AdamW optimizer, which is the normal Adam optimizer combined with an additional weight decay variable, is used (default value: 10^{-2}). AdamW decouples the weight decay from the size of the learning rate, making it only proportional to the weight itself. It has also been proven to give better generalizing models (Loschchillow & Hutter, 2019).

2.4 Modularity maximization

In order to investigate the robustness of the network, the neural network was trained multiple times with different initializations. For each initialization, we computed the activation of the three features in the final hidden layer of the SNN, for every subject. For this analysis, the input correlation matrix was based on all timepoints of each participant. Then, in order to identify shared features across different initialization, a clustering technique, named modularity maximization, was used to group the features of the different networks. Modularity maximization extracts communities from large networks. When two features are combined and the modularity increases, the features are part of the same community (Rubinov & Sporns, 2010). The MATLAB community Louvain function of Rubinov and Sporns (2010) was used, which is an iterative algorithm that maximizes the within-module edges and minimizes the between-modules edges. The algorithm was executed with a gamma of different values in a range of 0.5-3. The exact value of gamma will be chosen based on the number of clusters resulting from that gamma value, and the change in the number of clusters based on increasing the value of gamma.

Different initializations of the same network might learn the same features with a different sign (positive/negative), or even completely different hidden layer activations, despite the performance being relatively similar (Mehrer et al., 2020). Therefore, before running the modularity maximization, we investigated if flipping the sign would increase the similarity to features learned in other network initializations. First, for every feature separately, the feature scores over subjects were inverted. Then, the correlation over the features was computed again with the inverted feature value. If the sum of this correlation matrix is larger than of the correlation matrix when the sign of that feature was not inverted, the changed sign of the feature was kept. This procedure was performed for every feature and repeated for all features until no feature changed anymore.

2.5 Occlusion analysis

In order to visualize the hidden activations, an occlusion analysis was performed. To obtain a representative input for the occlusion analyses, the correlation matrix of the complete time course of rs-fMRI data is computed for every participant. Then these correlation matrices are averaged across participants. This is used as the input of the SNN, which is then used to compute the output, which are the activations of hidden layer 5. However, when the hidden layer activation is inverted (see *2.4 Modularity maximization*), the weight of the feature is also flipped here. Then the occlusion analysis is performed. One specific element in the correlation matrix is set to 1000. The value 1000 was chosen, since two ROIs can have a correlation of 0. This would not give the contrast we need to see the change in final activation values. Next, this full input matrix is used as the input of the model, resulting in a new output matrix. Then, the element is restored to its original value. By computing the difference between the original output and the new output, we can see how the output changes based on that one input element. This is then done for every single element of the input.

2.6 Link with behavior

The HCP dataset does not only contain imaging data, but also behavioral data. These data were linked to the features learned by the SNN. The Pearson correlation coefficient was computed between the three feature scores per subject and the behavioral tests from the NIH Toolbox and the Penn tests. Then, only the correlations between the features and the cognitive scores that are significant, meaning correlations with a p-value smaller than 0.05 after false discovery rate (FDR) correction, were interpreted.

The behavioral tests are the following:

- The picture sequence memory test to measure episodic memory (Dikmen et al., 2014).
- The Penn word memory test (total number of correct responses) to measure verbal episodic memory (Gur et al. 2001).
- The list sorting test, where working memory is measured by the accuracy on both the visually- and orally-presented stimuli conditions (Tulsky et al., 2014).
- The Penn progressive matrices, where the number of correct responses is a measure of fluid intelligence (Bilker et al., 2012).
- The variable short Penn line orientation test (total number of correct responses) measures spatial orientation processing (Gur et al. 2001).
- The dimensional change card sort test is a measure of cognitive flexibility (Bialystok et al., 2004).
- The pattern completion processing speed test, which, as the name says, measures the speed of processing (Liu et al., 2016).
- The cognitive function composite score is derived by combining the scores of fluid (Penn progressive matrices) and crystallized (oral reading recognition test) cognition (Bilker et al., 2012; Weintraub et al., 2013)
- Language skills were measured by the language/reading decoding test and the language/vocabulary comprehension task (Gershon et al., 2013).
- The Penn emotion recognition test was used to measure emotion recognition (Gur et al. 2001).

3. Results

3.1 Model performance

Multiple models are trained in order to investigate the generalizability of the network. The training phase of each model is terminated when the training accuracy did no longer increase. This resulted in 9 models, which all achieved their highest training accuracy after 5 or 6 epochs. The training and validation accuracies per trained network are in Table 1. The mean training accuracy is 99.95%. The mean validation accuracy of all networks is 93.66%.

Table 1: Training and validation accuracy per model. The first row contains the training accuracy percentages for every trained model. The second row contains the validation accuracy percentages for every trained model. The third row contains the last epoch for which the validation accuracy has increased.

Model	**1**	**2**	**3**	**4**	**5**	**6**	**7**	**8**	**9**
Training Accuracy	99.98%	99.99%	99.97%	100%	99.68%	100%	99.99%	100%	100%
Validation Accuracy	93.38%	93.46%	93.41%	93.85%	93.42%	93.86%	93.86%	93.85%	93.85%
Epoch	5	6	5	5	6	5	6	5	5
Autoencoder Performance	60.53%	60.53%	60.52%	60.47%	60.53%	60.53%	60.53%	60.53%	60.43%

The performance of the autoencoder was measured by computing the Pearson's correlation coefficient between the original input and the reconstructed input for every subject. This was then averaged over subjects (see Table 1). Then, in order to investigate whether the autoencoder is able to reconstruct individual differences, the correlation between the input connectivity profiles per subject is computed, just as the correlation between the reconstructions over subjects are computed. Then, the subjects are sorted based on their correlation with other subjects (see Figure 3). The more similar these matrices, the better the autoencoder has captured the individual differences between subjects. As can be seen in Figure 3, the autoencoder did not really capture the individual differences between subjects.

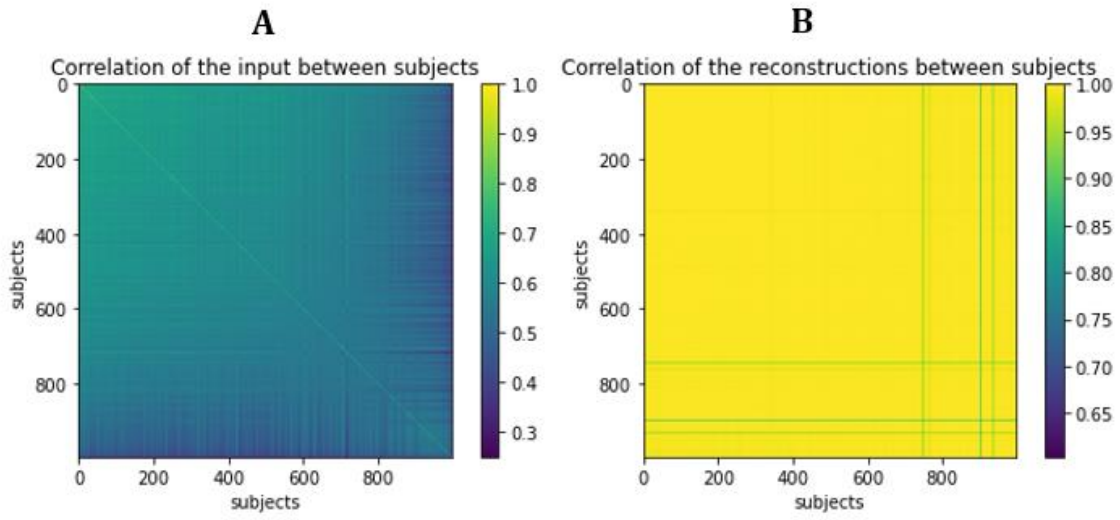

Figure 3: A) Correlation matrix of the input matrix between subjects. B) Correlation matrix of the autoencoder output between subjects.

3.2 Modularity maximization

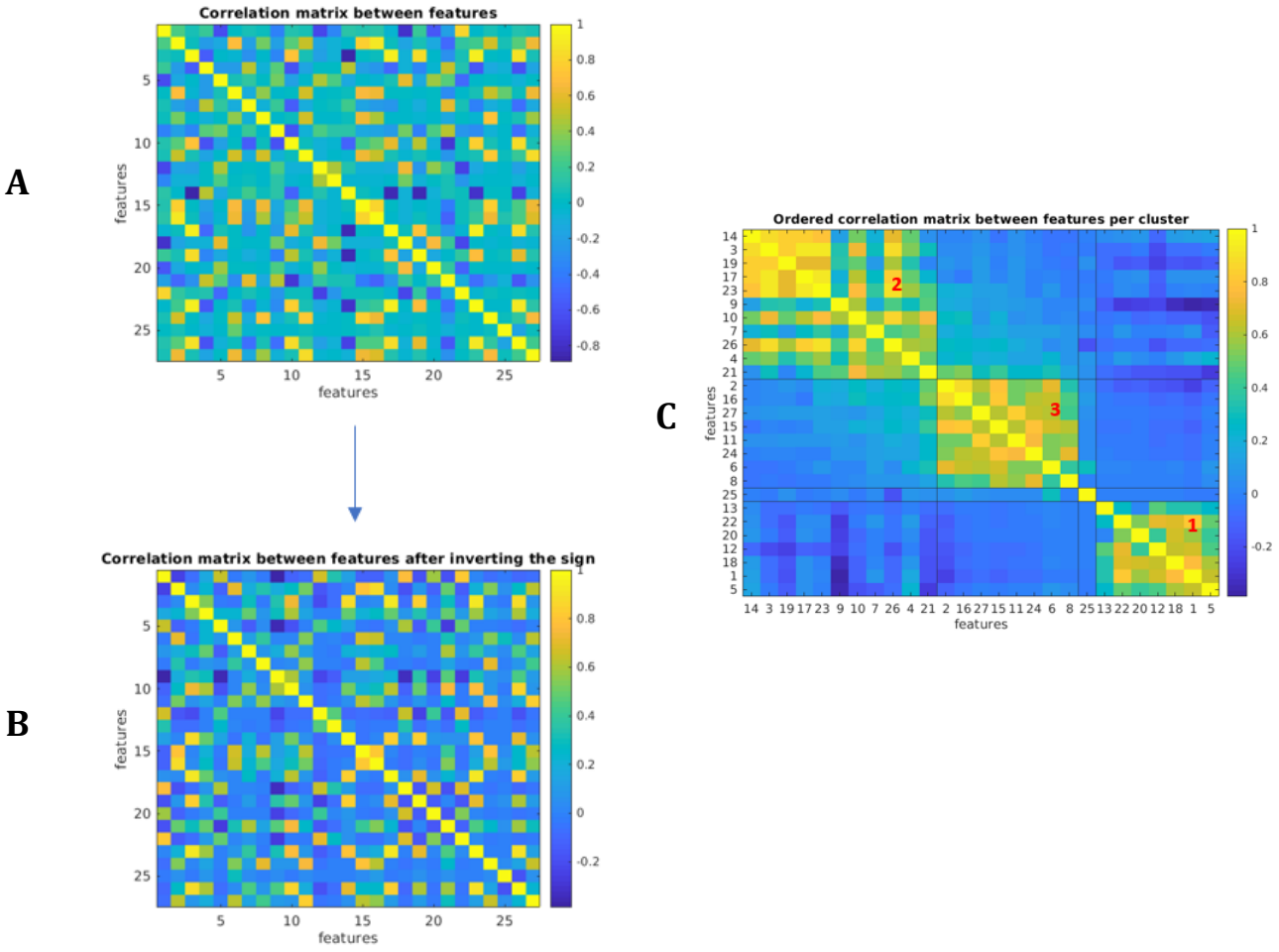

Figure 4: Correlation matrices between the features. A) The correlation matrix between the different features over subjects. B) The correlation matrix between different features over subjects, after the signs are inverted when the correlation increased (See 2.4 Modularity maximization). C) The correlation matrix between the features after the modularity maximization algorithm. The features are ordered per cluster according to the modularity maximization algorithm. The number of the cluster is indicated in red, while the vertical and horizontal lines indicate the end of the cluster and a beginning of a new cluster.

Next, the modularity maximization algorithm divided the features of different models into clusters. As indicated in the methods section, the signs of the features were first inverted if this increased the sum of the correlation matrix. Figure 4A shows the correlation matrix of the features before and Figure 4B shows the correlation matrix after inverting the signs. Then, this correlation matrix is used as the input of the modularity maximization algorithm. Based on the value of gamma, a different amount of clusters were found, ranging from 3 (gamma=1) to 6 (gamma=1.5/1.6). Higher values of gamma resulted in more clusters that included only one feature. Therefore, only clusters with gamma is 1.0, 1.2, 1.4 and 1.6 will be showed. Table 2 shows the features of the models and their corresponding clustering index, for the different values of gamma. The first feature of model 9 was not clustered with any other feature when the number of clusters exceeds 3 (See Table 2, the pink column) and showed weak correlation to all other features (see Figure 4C). Therefore, this feature is not incorporated in the next analyses steps. Our aim was to identify features that were recurrent across many different initializations of the model. That is why we choose a gamma of value 1.2, resulting in 3 components. Cluster 1 contains

one feature from almost every model (except from model 7). These features are the same for the different gamma values. Therefore, these features are identified as component 1. Cluster 3 contains one features from almost every model (excepts from model 3 and 9), being combined as component 2. Cluster 2 is separated into multiple clusters when gamma is increased.

Table 2: Cluster indices for every feature for increasing gamma values. Blue-coloured squares indicate that the feature is part of cluster 1. Orange-coloured squares indicate that the feature is part of cluster 2. Green-coloured squares indicate that the feature is part of cluster 3. Feature 1 of model 9, which is coloured in pink, does not belong to a cluster with other features for gamma higher than 1.0.

Model	**1**			**2**			**3**			**4**			**5**			**6**			**7**			**8**			**9**		
Features	**1**	**2**	**3**	**1**	**2**	**3**	**1**	**2**	**3**	**1**	**2**	**3**	**1**	**2**	**3**	**1**	**2**	**3**	**1**	**2**	**3**	**1**	**2**	**3**	**1**	**2**	**3**
GAMMA=1.0	3	1	2	2	3	1	2	1	2	2	1	3	3	2	1	1	2	3	2	3	2	3	2	1	1	2	1
GAMMA=1.2	3	1	2	2	3	1	2	1	2	2	1	3	3	2	1	1	2	3	2	3	2	3	2	1	4	2	1
GAMMA=1.4	3	1	2	4	3	1	4	1	2	2	1	3	3	2	1	1	2	3	2	3	4	3	2	1	5	2	1
GAMMA=1.6	3	1	2	5	3	1	4	1	4	4	1	3	3	2	1	1	2	3	2	3	4	3	2	1	6	2	1

3.3 Occlusion analysis

Then, we wanted to combine the features of the same clusters and visualize these results. An occlusion analysis is performed on every feature. The resulting occlusion matrices are then z-scored, such that every occlusion matrix has the same scale. Next, the occlusion matrices of the features that belong to the same cluster are averaged and again z-scored with a threshold of z>1. The occlusion matrices of the clusters can be seen in Figure 5.

A

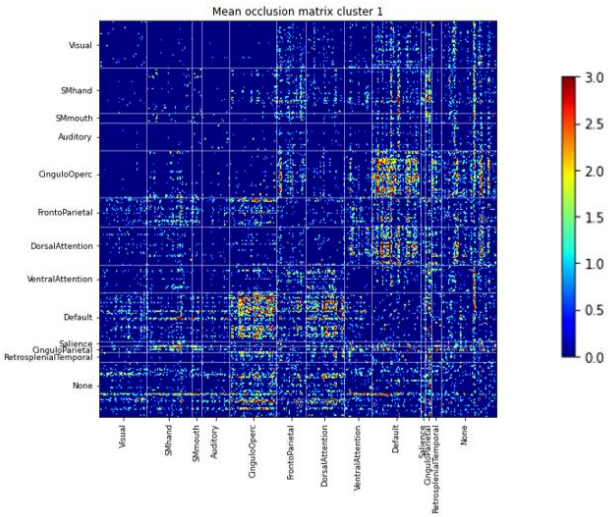

B

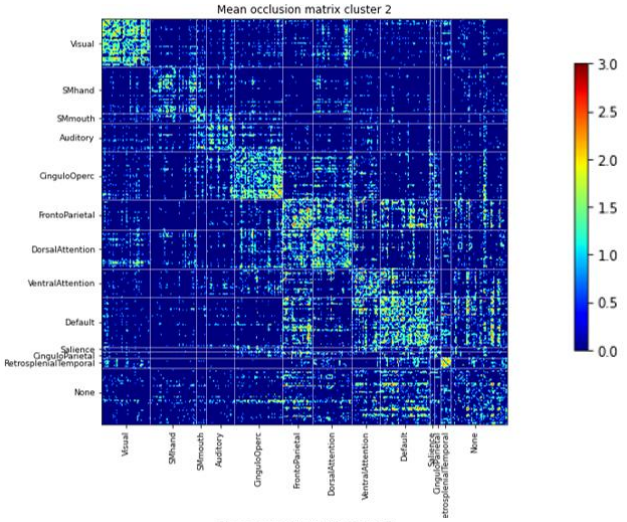

C

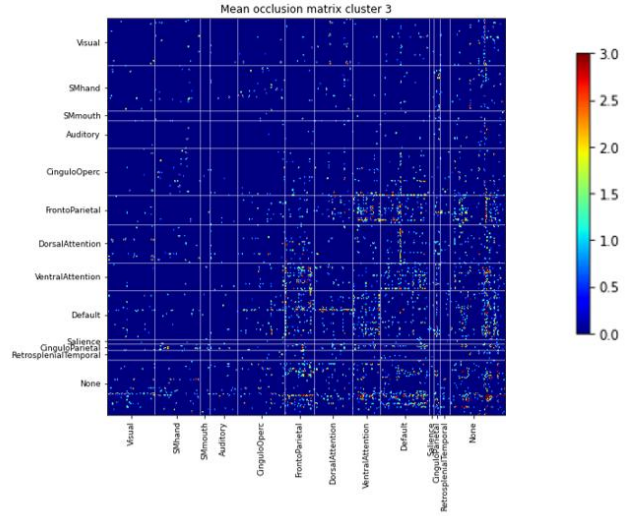

Figure 5: Mean occlusion matrix of features belonging to the different clusters, showing the Pearson correlation coefficient between the ROIs. A) Component 1: mean occlusion matrix of features belonging to cluster 1. B) Component 2: mean occlusion matrix of features belonging to cluster 2. C) Component 3: mean occlusion matrix of features belonging to cluster 3.

Component 1 (Figure 5A) is driven by the connections between the default mode network, cinguloopercular network and the dorsal attention network, and a lower number of connections with the somatosensory network.

Component 2 is affected by high within-network connections, as can be seen on the diagonal of Figure 5B. Here, the component is driven by connections between ROIs in the same network. There are also some connections between the frontoparietal network and the default mode network. Then, the component is slightly affected by connections belonging to different networks.

For component 3 (Figure 5C) the connections between ROIs are lower and less consistent than for the previous components. Component 3 is affected by the frontoparietal network, the dorsal and ventral attention network, and the default mode network. The component is also affected by some ROIs that do not belong to any network (corresponding to the 'None' row and column in Figure 5C), which have connections with all other networks, including themselves.

3.4 Link with behavior

The full table of correlations between the feature scores per subject and the cognitive scores per subject can be seen in Appendix A, where the significant correlations are in bold. Here, we will only discuss the correlations that are significant. First, Figure 6 shows the significant correlations of all features with the cognitive scores per test. Here, it can be seen that for some features, there are a lot of significant correlations with the cognitive scores, while for others, there are (almost) none.

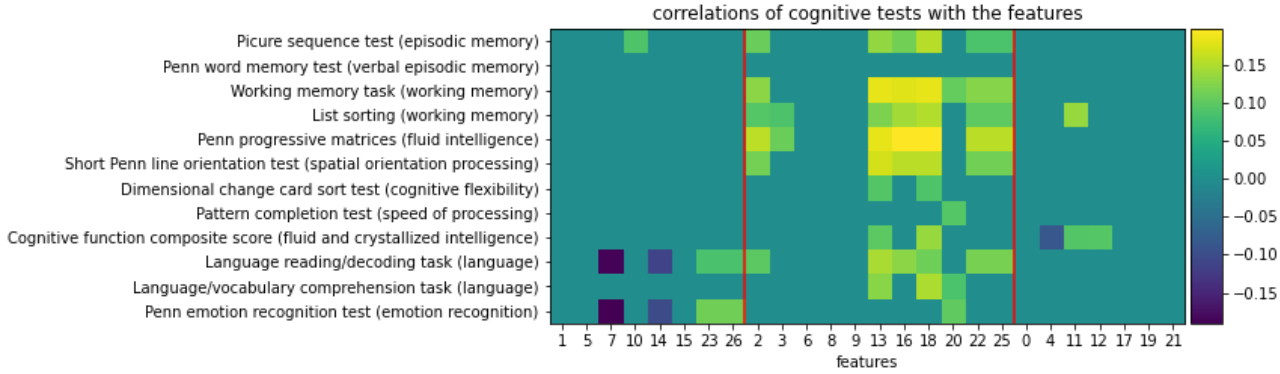

Figure 6: Significant correlations between the cognitive tests and all features. The left column contains the correlations for the features of cluster one, the middle column for cluster 2 and the right column for cluster 3.

For cluster 1, some features have a significant correlation with the cognitive scores (see the left column of Figure 6). Features 7, 14, 23 and 26 have significant correlations with language reading and emotion recognition. Only feature 10 has a significant correlation with episodic memory.

In cluster 2, feature 2, 13, 16, 18, 22 and 25 have a significant correlation with episodic memory (see Figure 6, middle part). Feature 2, 3, 13, 16, 18, 20, 22 and 25 have a significant correlation with working memory. Feature 2, 3, 13, 16, 18, 22 and 25 have a significant correlation with fluid intelligence, while only feature 13 and 18 have a significant correlation with both fluid and crystallized intelligence. The last two also have a significant correlation with cognitive flexibility. Feature 2, 13, 16, 18, 22 and 25 have a significant correlation with spatial orientation processing. Feature 2, 13, 16, 18, 22 and 25 have a significant correlation with language reading, and feature 13, 18 and 20 have a significant correlation with language comprehension. Only feature 20 has a significant correlation with emotion recognition and speed of processing.

For cluster 3, there are barely any significant correlations between the cognitive test scores and the features (See Figure 6, right column. Feature 4, 11 and 12 have a significant correlation with fluid and crystallized intelligence. Feature 11 also has a significant correlation with working memory.

4. Discussion

In this study, we investigated whether we could identify features that are a low-dimensional representation of inter-individual variability of brain function. Here, we found 3 components.

The first component is driven by higher-level brain networks, such as the default mode network, the cinguloopercular network and the dorsal attention network. These higher-order networks have been proven to by important in inter-individual variability before (Mohr & Nagel, 2010; Kanai & Rees, 2011). The importance of the default mode network is not a surprise, since we are using resting-state fMRI data and the default mode network is known for its activation during resting

state (Van den Heuvel & Hulshoff Pol, 2010). These networks were also found in other functional connectivity fingerprint studies that were discussed before. Gratton et al. (2018) found individual variability in the cinguloopercular, frontoparietal and attention networks. The dorsal attention network was predicted from individuals' functional connectivity fingerprints. Then, the default mode network and the dorsal attention network have been shown to be important for externally and internally directed cognition (Qian et al., 2020). They are having an anti-correlation, where they compete for endogenous and exogenous cognitive activities (Franzmeier et al., 2016). The anti-correlation between the default mode network and the dorsal attention network has also been shown to be important in cognitive function in older adults (Franzmeier et al., 2016). Here, lower levels of DMN-DAN crosstalk result in lower memory performance (Franzmeier et al., 2016; Avelar-Pereira et al., 2017). Unfortunately, we did not find a correlation between this component and working memory or episodic memory. We did find a correlation with language reading and emotion recognition.

Then, the second component is driven by intra-network relations. The highest contributions were for connections between ROIs belonging to the same networks. Disrupted intra-network connectivity has been related to numerous disorders, such as depression (Manoliu et al., 2014), Alzheimer's disease (Wang et al., 2015) and schizophrenia (Houck et al., 2017) and to changes due to aging (La et al., 2015). We also see correlations with numerous cognitive functions, such as episodic and working memory, spatial orientation processing, cognitive flexibility, intelligence, language, and slightly with speed of processing and emotion recognition. This shows that within-network connectivity is an important aspect of cognitive function, with impairments of different intra-network connections leading to different types of cognitive problems.

The third component was also driven by the frontoparietal network, the attention networks and the default mode network, but this was less prominent than for component 1. Here, the component was also slightly driven by the ROIs that did not belong to any network. Then, the component only had a correlation with fluid and crystallized intelligence. The interaction between the frontoparietal regions and the default mode network have been suggested to be important for fluid intelligence (Santarnecchi et al., 2017). Finn et al. (2015) found that the frontoparietal network was most important for identifying individuals and the connectivity profiles also predicted levels of fluid intelligence.

We trained a Siamese neural network to determine whether the two inputs are resting-state fMRI data from a different or the same person. The SNN has a performance of 93%. Performance of chance level is 50%, meaning that we reached high accuracy. Here, we see that our accuracy is slightly lower than the results of Yoo et al. (2019), who had a performance around 97% for their multivariate approach. However, they used a second dataset, and, for their univariate approaches, only an accuracy of 58% was obtained. Byrge et al. (2019) showed that with only 0.3% of all functional connections, an accuracy of 98% can be achieved when combining resting scan data together with video watching scan data. Then, the correlation between the input matrix per subject and the reconstruction of the autoencoder of that input was approximately 60%. So, the reconstructions of the input were for above chance level. However, the autoencoder was not able to capture the individual differences between people in the reconstructions.

Next, we see that the performance of the network remains stable when training it with a different initializations, since the performance of each network is approximately 93%. However, the features learned by the network are different. This confirms the conclusion of Mehrer et al. (2020), where they showed that different initializations can lead to different high-level feature, despite the similar accuracies of the models. Since these features were not equal, we used a modularity maximization algorithm to cluster the features of the different models. Here, clustering is one way to make sense

of the found features, but there are other techniques that one might use in order to make sense of the huge feature space such as multidimensional scaling, or principal component analysis.

Not only the initialization, but also the network architecture might be important for finding different features. In this study, we only used one type of network architecture. In the future, it would be interesting to see how changing this architecture would affect the components found and the correlations of these components with behavior. Also, the choice of dataset could be important.

To conclude, by training a Siamese neural network on resting state fMRI data, the network can learn to discriminate whether the inputs are from the same person or not with high accuracy. The features then learned by the network can be linked to large-scale brain networks and the subjects' cognitive scores.

5. References

Avelar-Pereira, B., Bäckman, L., Wåhlin, A., Nyberg, L., & Salami, A. (2017). Age-related differences in dynamic interactions among default mode, frontoparietal control, and dorsal attention networks during resting-state and interference resolution. *Frontiers in Aging Neuroscience*, *9*, 152.

Amboni, M., Tessitore, A., Esposito, F., Santangelo, G., Picillo, M., Vitale, C., ... & Barone, P. (2015). Resting-state functional connectivity associated with mild cognitive impairment in Parkinson's disease. *Journal of neurology*, *262*(2), 425-434.

Balsters, J. H., O'Connell, R. G., Galli, A., Nolan, H., Greco, E., Kilcullen, S. M., ... & Robertson, I. H. (2013). Changes in resting connectivity with age: a simultaneous electroencephalogram and functional magnetic resonance imaging investigation. *Neurobiology of Aging*, *34*(9), 2194-2207.

Beckmann, C. F., DeLuca, M., Devlin, J. T., & Smith, S. M. (2005). Investigations into resting-state connectivity using independent component analysis. *Philosophical Transactions of the Royal Society B: Biological Sciences*, *360*(1457), 1001-1013.

Bialystok, E., & Martin, M. M. (2004). Attention and inhibition in bilingual children: Evidence from the dimensional change card sort task. *Developmental science*, *7*(3), 325-339.

Bilker, W. B., Hansen, J. A., Brensinger, C. M., Richard, J., Gur, R. E., & Gur, R. C. (2012). Development of abbreviated nine-item forms of the Raven's standard progressive matrices test. *Assessment*, *19*(3), 354-369.

Byrge, L., & Kennedy, D. P. (2019). High-accuracy individual identification using a "thin slice" of the functional connectome. *Network Neuroscience*, *3*(2), 363-383.

Chen, B., Xu, T., Zhou, C., Wang, L., Yang, N., Wang, Z., ... & Weng, X. C. (2015). Individual variability and test-retest reliability revealed by ten repeated resting-state brain scans over one month. *PloS one*, *10*(12), e0144963.

Chen, S., & Hu, X. (2018). Individual identification using the functional brain fingerprint detected by the recurrent neural network. *Brain connectivity*, *8*(4), 197-204.

Damoiseaux, J. S., Rombouts, S. A. R. B., Barkhof, F., Scheltens, P., Stam, C. J., Smith, S. M., & Beckmann, C. F. (2006). Consistent resting-state networks across healthy subjects. *Proceedings of the national academy of sciences*, *103*(37), 13848-13853.

da Silva Castanheira, J., Orozco, H. D., Misic, B., & Baillet, S. (2021). MEG, myself, and I: individual identification from neurophysiological brain activity. *bioRxiv*.

Demeter, D. V., Engelhardt, L. E., Mallett, R., Gordon, E. M., Nugiel, T., Harden, K. P., ... & Church, J. A. (2020). Functional connectivity fingerprints at rest are similar across youths and adults and vary with genetic similarity. *Iscience*, *23*(1), 100801.

Dikmen, S. S., Bauer, P. J., Weintraub, S., Mungas, D., Slotkin, J., Beaumont, J. L., ... & Heaton, R. K. (2014). Measuring episodic memory across the lifespan: NIH toolbox picture sequence memory test. *Journal of the International Neuropsychological Society: JINS*, *20*(6), 611.

Dimitri, G. M., Spasov, S., Duggento, A., Passamonti, L., Lio, P., & Toschi, N. (2021). Multimodal image fusion via deep generative models. *bioRxiv*.

Finn et al. (2015). Functional connectome fingerprinting: identifying individuals using patterns of brain connectivity. *Nature Neuroscience, 18*, 1664–1671.

Franzmeier, N., Buerger, K., Teipel, S., Stern, Y., Dichgans, M., Ewers, M., & Alzheimer's Disease Neuroimaging Initiative (ADNI. (2017). Cognitive reserve moderates the association between functional network anti-correlations and memory in MCI. *Neurobiology of Aging*, *50*, 152-162.

Friston, K. J. (1994). Functional and effective connectivity in neuroimaging: a synthesis. *Human brain mapping*, *2*(1-2), 56-78.

Friston, K. J. (2011). Functional and effective connectivity: a review. *Brain connectivity*, *1*(1), 13-36.

Gordon, E. M., Laumann, T. O., Adeyemo, B., Gilmore, A. W., Nelson, S. M., Dosenbach, N. U., & Petersen, S. E. (2017). Individual-specific features of brain systems identified with resting state functional correlations. *Neuroimage*, *146*, 918-939.

Geerligs, L., Renken, R. J., Saliasi, E., Maurits, N. M., & Lorist, M. M. (2014). A brain-wide study of age-related changes in functional connectivity. *Cerebral cortex*, *25*(7), 1987-1999.

Gershon, R. C., Slotkin, J., Manly, J. J., Blitz, D. L., Beaumont, J. L., Schnipke, D., Wallner-Allen, K., Golinkoff, R. M., Gleason, J. B., Hirsh-Pasek, K., Adams, M. J., & Weintraub, S. (2013). IV. NIH Toolbox Cognition Battery (CB): measuring language (vocabulary comprehension and reading decoding). *Monographs of the Society for Research in Child Development*, *78*(4), 49–69. https://doi.org/10.1111/mono.12034

Gratton et al. (2018). Functional Brain Networks are dominated by stable group and individual factors, not cognitive or daily variation. *Neuron, 98*(2), 439–452.

Gur, R. C., Ragland, J. D., Moberg, P. J., Turner, T. H., Bilker, W. B., Kohler, C., ... & Gur, R. E. (2001). Computerized neurocognitive scanning:: I. Methodology and validation in healthy people. *Neuropsychopharmacology*, *25*(5), 766-776.

Horien, C., Shen, X., Scheinost, D., & Constable, R. T. (2019). The individual functional connectome is unique and stable over months to years. *Neuroimage*, *189*, 676-687.

Houck, J. M., Çetin, M. S., Mayer, A. R., Bustillo, J. R., Stephen, J., Aine, C., ... & Calhoun, V. D. (2017). Magnetoencephalographic and functional MRI connectomics in schizophrenia via intra-and inter-network connectivity. *Neuroimage*, *145*, 96-106.

Kanai, R., & Rees, G. (2011). The structural basis of inter-individual differences in human behaviour and cognition. *Nature Reviews Neuroscience*, *12*(4), 231-242.

Koch, G., Zemel, R., & Salakhutdinov, R. (2015). Siamese neural networks for one-shot image recognition. *In ICML deep learning workshop* (Vol. 2).

La, C., Mossahebi, P., Nair, V. A., Bendlin, B. B., Birn, R., Meyerand, M. E., & Prabhakaran, V. (2015). Age-related changes in inter-network connectivity by component analysis. *Frontiers in aging neuroscience*, *7*, 237.

Langer, N., Pedroni, A., Gianotti, L. R., Hänggi, J., Knoch, D., & Jäncke, L. (2012). Functional brain network efficiency predicts intelligence. *Human brain mapping, 33*(6), 1393-1406.

Liu, K. Y., Gould, R. L., Coulson, M. C., Ward, E. V., & Howard, R. J. (2016). Tests of pattern separation and pattern completion in humans—A systematic review. *Hippocampus*, *26*(6), 705-717.

Loshchilov, I. & Hutter, F. (2019) Decoupled Weight Decay Regularization. *7th International Conference on Learning Representations, New Orleans*, 6-9 May 2019. https://dblp.org/rec/conf/iclr/LoshchilovH19.html

Lynall, M. E., Bassett, D. S., Kerwin, R., McKenna, P. J., Kitzbichler, M., Muller, U., & Bullmore, E. (2010). Functional connectivity and brain networks in schizophrenia. *Journal of Neuroscience*, *30*(28), 9477-9487.

Manoliu, A., Meng, C., Brandl, F., Doll, A., Tahmasian, M., Scherr, M., ... & Sorg, C. (2014). Insular dysfunction within the salience network is associated with severity of symptoms and aberrant inter-network connectivity in major depressive disorder. *Frontiers in human neuroscience*, *7*, 930.

Mansour L.S., Tian Y., Yeo B.T. T., Cropley V., Zalesky A.,(2021) High-resolution connectomic fingerprints: mapping neural identity and behavior, *NeuroImage*, doi: https://doi.org/10.1016/j.neuroimage.2020.117695

Mars, R. B., Passingham, R. E., & Jbabdi, S. (2018). Connectivity fingerprints: from areal descriptions to abstract spaces. *Trends in cognitive sciences, 22*(11), 1026-1037.

Mehrer, J., Spoerer, C. J., Kriegeskorte, N., & Kietzmann, T. C. (2020). Individual differences among deep neural network models. *Nature communications*, *11*(1), 1-12.

Miranda-Dominguez, O., Mills, B. D., Carpenter, S. D., Grant, K. A., Kroenke, C. D., Nigg, J. T., & Fair, D. A. (2014). Connectotyping: model based fingerprinting of the functional connectome. *PloS one*, *9*(11), e111048.

Mohr, P. N., & Nagel, I. E. (2010). Variability in brain activity as an individual difference measure in neuroscience?. *Journal of Neuroscience*, *30*(23), 7755-7757.

Moussa, M. N., Vechlekar, C. D., Burdette, J. H., Steen, M. R., Hugenschmidt, C. E., & Laurienti, P. J. (2011). Changes in cognitive state alter human functional brain networks. *Frontiers in human neuroscience*, *5*, 83.

Mueller, S., Wang, D., Fox, M. D., Yeo, B. T., Sepulcre, J., Sabuncu, M. R., ... & Liu, H. (2013). Individual variability in functional connectivity architecture of the human brain. *Neuron*, *77*(3), 586-595.

Osher, D. E., Brissenden, J. A., & Somers, D. C. (2019). Predicting an individual's dorsal attention network activity from functional connectivity fingerprints. *Journal of neurophysiology*, *122*(1), 232-240.

Qian, S., Zhang, J., Yan, S., Shi, Z., Wang, Z., & Zhou, Y. (2020). Disrupted Anti-correlation Between the Default and Dorsal Attention Networks During Hyperthermia Exposure: An fMRI Study. *Frontiers in Human Neuroscience*, *14*, 473.

Santarnecchi, E., Emmendorfer, A., Tadayon, S., Rossi, S., Rossi, A., & Pascual-Leone, A. (2017). Network connectivity correlates of variability in fluid intelligence performance. *Intelligence*, *65*, 35-47.

Smith, S. M., Fox, P. T., Miller, K. L., Glahn, D. C., Fox, P. M., Mackay, C. E., ... & Beckmann, C. F. (2009). Correspondence of the brain's functional architecture during activation and rest. *Proceedings of the national academy of sciences*, *106*(31), 13040-13045.

Smith, S. M., Vidaurre, D., Beckmann, C. F., Glasser, M. F., Jenkinson, M., Miller, K. L., ... & Van Essen, D. C. (2013). Functional connectomics from resting-state fMRI. *Trends in cognitive sciences, 17*(12), 666-682.

Smitha, K. A., Akhil Raja, K., Arun, K. M., Rajesh, P. G., Thomas, B., Kapilamoorthy, T. R., & Kesavadas, C. (2017). Resting state fMRI: A review on methods in resting state connectivity analysis and resting state networks. *The neuroradiology journal*, *30*(4), 305-317.

Sripada, C., Angstadt, M., Rutherford, S., Kessler, D., Kim, Y., Yee, M., & Levina, E. (2019). Basic units of inter-individual variation in resting state connectomes. *Scientific reports*, *9*(1), 1-12.

Tulsky, D. S., Carlozzi, N., Chiaravalloti, N. D., Beaumont, J. L., Kisala, P. A., Mungas, D., ... & Gershon, R. (2014). NIH Toolbox Cognition Battery (NIHTB-CB): The list sorting test to measure working memory. *Journal of the International Neuropsychological Society: JINS*, *20*(6), 599.

Valizadeh, S. A., Riener, R., Elmer, S., & Jäncke, L. (2019). Decrypting the electrophysiological individuality of the human brain: Identification of individuals based on resting-state EEG activity. *NeuroImage*, *197*, 470-481.

Van Essen, D. C., Smith, S. M., Barch, D. M., Behrens, T. E., Yacoub, E., Ugurbil, K., & Wu-Minn HCP Consortium. (2013). The WU-Minn human connectome project: an overview. *Neuroimage*, *80*, 62-79.

Van Den Heuvel, M. P., & Pol, H. E. H. (2010). Exploring the brain network: a review on resting-state fMRI functional connectivity. *European neuropsychopharmacology, 20*(8), 519-534.

Voorn, M. (2020). *Underlying features of inter-individual variability in brain function* (Master's thesis).

Wang, K., Liang, M., Wang, L., Tian, L., Zhang, X., Li, K., & Jiang, T. (2007). Altered functional connectivity in early Alzheimer's disease: A resting-state fMRI study. *Human brain mapping*, *28*(10), 967-978.

Wang, P., Zhou, B., Yao, H., Zhan, Y., Zhang, Z., Cui, Y., ... & Jiang, T. (2015). Aberrant intra-and inter-network connectivity architectures in Alzheimer's disease and mild cognitive impairment. *Scientific reports*, *5*(1), 1-12.

Weintraub, S., Bauer, P. J., Zelazo, P. D., Wallner-Allen, K., Dikmen, S. S., Heaton, R. K., Tulsky, D. S., Slotkin, J., Blitz, D. L., Carlozzi, N. E., Havlik, R. J., Beaumont, J. L., Mungas, D., Manly, J. J., Borosh, B. G., Nowinski, C. J., & Gershon, R. C. (2013). I. NIH Toolbox Cognition Battery (CB): introduction and pediatric data. *Monographs of the Society for Research in Child Development*, *78*(4), 1–15. https://doi.org/10.1111/mono.12031

Yoo, K., Rosenberg, M. D., Noble, S., Scheinost, D., Constable, R. T., & Chun, M. M. (2019). Multivariate approaches improve the reliability and validity of functional connectivity and prediction of individual behaviors. *Neuroimage*, *197*, 212-223.

Zeng, L. L., Shen, H., Liu, L., Wang, L., Li, B., Fang, P., ... & Hu, D. (2012). Identifying major depression using whole-brain functional connectivity: a multivariate pattern analysis. *Brain*, *135*(5), 1498-1507.

Zhang, C., Liu, W., Ma, H., & Fu, H. (2016). Siamese neural network based gait recognition for human identification. *IEEE International Conference on Acoustics, Speech and Signal Processing (ICASSP)*, 2016, pp. 2832-2836, doi: 10.1109/ICASSP.2016.7472194.

Appendix A

The correlations between the features scores over subjects and the cognitive scores per subject. The tests are indicated with a letter, which are depicted at the end Appendix A. Correlations in bold are significant with a p-value smaller than 0.05 after FDR correction.

		model 1			model 2			model 3	
	feat 1	feat 2	feat 3	feat 1	feat 2	feat 3	feat 1	feat 2	feat 3
a	-0,00631	0,041811	**0,10913**	0,049671	-0,00679	0,015863	0,045134	0,050854	0,024052
b	0,033992	0,001353	0,040939	0,00651	0,041792	0,029223	-0,02762	-0,00845	-0,02728
c	0,021876	-0,03878	**0,129322**	0,037427	0,018194	-0,03503	-0,04731	-0,02176	-0,04086
d	-0,05929	-0,02809	**0,095729**	**0,089848**	-0,07401	-0,00551	0,024716	-0,04735	0,045253
e	0,005612	0,017397	**0,158214**	**0,110392**	0,028069	0,059576	0,030353	-0,00642	0,038749
f	0,025758	0,028542	**0,116162**	0,064388	0,012406	0,006442	-0,00449	0,021766	-0,03778
g	0,047917	0,003509	0,04873	0,05553	0,018286	-0,01201	-0,05276	0,019943	-0,03195
h	0,044909	-0,07721	0,027913	-0,01554	0,025193	-0,04203	-0,04063	-0,03016	-0,04173
i	-0,02627	-0,01009	0,067765	0,074751	**-0,08566**	0,000591	-0,02537	-0,01058	0,028485
j	0,046516	-0,04945	**0,099066**	0,052321	0,042375	-0,0676	0,018831	**-0,18634**	-0,03567
k	0,055812	-0,03596	0,062084	0,070518	0,035144	-0,00926	-0,01975	-0,02449	-0,01372
l	0,035634	-0,04563	-0,01524	-0,05979	0,018587	-0,07815	-0,04687	**-0,19033**	-0,05918

		model 4			model 5			model 6	
	feat 1	feat 2	feat 3	feat 1	feat 2	feat 3	feat 1	feat 2	feat 3
a	0,047901	**0,09**	0,04334	-0,04425	**0,134856**	0,030876	0,027643	**0,115063**	0,009728
b	-0,00216	0,041395	-0,00306	-0,03183	0,057928	0,008037	-0,00586	0,057947	0,027891
c	-0,00284	0,032641	0,005567	-0,04518	**0,183273**	-0,02629	-0,04604	**0,17772**	0,044
d	0,012185	-0,01302	**0,137782**	0,044494	**0,12073**	-0,04799	-0,05529	**0,143188**	-0,06741
e	0,066801	0,069465	0,032642	-0,01108	**0,182301**	0,010884	0,01387	**0,197021**	0,034815
f	0,025366	0,03357	0,048718	-0,00847	**0,173011**	0,04052	0,027894	**0,156528**	0,030567
g	-0,02901	0,01793	0,005331	-0,02408	**0,093406**	0,020316	0,009847	0,077893	0,026935
h	-0,05358	-0,05036	0,002605	-0,03625	0,065119	-0,06156	-0,07639	0,050239	0,028184
i	0,007399	0,013968	**0,094172**	**0,09519**	**0,099385**	-0,00644	0,006995	0,081958	-0,0632
j	0,04386	-0,03891	-0,01836	-0,03314	**0,148812**	**-0,11232**	-0,0336	**0,13073**	0,060439
k	-0,00672	0,000703	-0,01919	-0,00647	**0,129044**	-0,02133	0,024366	0,073665	0,054885
l	-0,05808	-0,07828	-0,02556	-0,02049	0,032095	**-0,10075**	-0,06003	0,0151	0,029359

		model 7			model 8			model 9	
	feat 1	feat 2	feat 3	feat 1	feat 2	feat 3	feat 1	feat 2	feat 3
a	**0,155006**	-0,022	0,019909	0,00401	**0,086985**	-0,04405	0,00401	**0,086985**	-0,04405
b	0,047334	0,011428	0,041681	-0,0525	0,056609	-0,0133	-0,0525	0,056609	-0,0133
c	**0,182738**	0,03637	**0,105823**	-0,04649	**0,127043**	-0,00757	-0,04649	**0,127043**	-0,00757
d	**0,152497**	-0,05381	0,039217	0,075292	**0,100765**	0,032413	0,075292	**0,100765**	0,032413
e	**0,197382**	0,034144	0,003541	-0,02831	**0,156811**	-0,04773	-0,02831	**0,156811**	-0,04773

f	**0,156507**	0,028641	0,042287	-0,00033	**0,114585**	-0,03519	-0,00033	**0,114585**	-0,03519
g	**0,090745**	-0,0026	0,060522	-0,05758	0,042458	-0,03054	-0,05758	0,042458	-0,03054
h	0,048901	0,055876	**0,095901**	-0,03816	-0,0009	0,034151	-0,03816	-0,0009	0,034151
i	**0,138024**	-0,02706	0,036212	0,029755	0,04712	-0,01705	0,029755	0,04712	-0,01705
j	**0,111732**	0,028926	0,012354	-0,05169	**0,1174**	**0,085443**	-0,05169	**0,1174**	**0,085443**
k	**0,149334**	0,025095	**0,087283**	-0,05353	0,056807	-0,02223	-0,05353	0,056807	-0,02223
l	0,012742	0,019737	**0,103248**	-0,02079	-0,00369	**0,112793**	-0,02079	-0,00369	**0,112793**

a Picture sequence test (episodic memory)

b Penn word memory test (verbal episodic memory)

c Working memory task (working memory)

d List sorting (working memory)

e Penn progressive matrices (fluid intelligence)

f Short Penn line orientation test (spatial orientation processing)

g Dimensional change card sort test (cognitive flexibility)

h Pattern completion test (speed of processing)

i Cognitive function composite score (fluid and crystallized intelligence)

j Language reading/decoding task (language)

k Language/vocabulary comprehension task (language)

l Penn emotion recognition test (emotion recognition)